Shallow granular flows

O. Bokhove[1] and A.R. Thornton[2]

1. Department of Applied Mathematics

2. Department of Applied Mathematics and Department of Mechanical Engineering

University of Twente, Enschede, 7500AE, The Netherlands

I. INTRODUCTION

Straightforward shallow granular flow consists of the movement of dry particulate material traveling in relatively thin layers over (inclined) topography. Often the fluidized material involved is more complex, consisting of a multiphase mixture of predominantly solid matter with an interstitial fluid filling the pore space. Small-scale laboratory experiments of glass beads or sand flowing down inclined chutes are an example of the dry case, which are performed to study idealized granular systems. In nature, the situation is often complicated by the presence of a fluid; examples include the collapse of water-saturated slopes into debris flows, or the flow of pyroclastic material into a river forming a lahar.

The fascination of shallow granular flows lies in their multi-facetted behavior. Particles are strongly forced down-slope by gravity, delivering energy to the system and allowing the particles to flow. This energy is balanced by losses through inelastic particle-particle collisions and frictional interaction with the substrate over which the particles are moving. After a short initialization process these two effects are approximately in balance and there is no net flow of energy into the system. We will see that, to leading order, a separate conservation of energy consideration will not be required to model these shallow flows. From a macro-scale viewpoint, the dynamics of fast granular flows are then akin to the fluid mechanics of shallow layers of

water with a free surface. A notable difference, in the granular case, is that the constitutive or closure laws for the bottom stress relations are generally unknown, except perhaps in very special cases. The separation between the macroscopic granular flow scales of interest and the microscopic scales, as given by the mean free path of granular particles, is much smaller than in molecular fluids; however, the continuum formulation for granular flows is still valid, even though less distinct. Depending on the particle size, the free surface in these fast shallow granular flows is clearly seen by eye to be grainy, on the macroscopic scale, and only exists in a statistical sense using space and/or time averages.

When gravitational forcing is small, the collective particle behavior is (quasi) static and concerns the realm of solid mechanics involving larger particle deformations, multiple simultaneous inter-particle contacts and force chains. Mixed continuum behavior arises in transient granular flows with static and dynamic zones. In all these cases micro-scale discrete particle methods (DPMs) form a useful tool. In DPMs the individual forces on all the particles are calculated and their positions updated via the integration of Newton's equations of motion. In DPMs, the deformation of the particles during collisions is simplified using a contact model to enhance computational speed (e.g., Van der Hoef 2006). We will limit ourselves to fluidized shallow granular flows in that the flow scales and speeds are small in one direction normal to the topography relative to the other directions. Hence, "depth-averaging" will be applied in the direction approximately normal to the terrain, to obtain leading-order models. For highly varying terrain, curvilinear coordinates will be required, but we will restrict attention to mildly undulating topography with one clearly defined average slope angle.

A typical industrial application of granular flows concerns the inflow of sinter, pellets and cokes, via a rotating inclined channel, into the blast furnace for iron-ore melting, at Corus

Hoogovens, IJmuiden, The Netherlands. These particles have different sizes and densities, and are also irregular in shape. In this situation particle segregation occurs, which is stimulated by the channel's rotation. Both the dynamics of the segregation and the motion of irregularly shaped particles are poorly understood problems. Comprehension of such problems is required to control these industrial flows, such that costly bottlenecks in the production process can be avoided. Study of these flows often provides insights in similar granular flows in the natural environment. A typical geological application concerns the 2005 landslide and debris flow after the collapse of a water saturated slope of pyroclastic material high on Tolimán Volcano in Guatemala. This debris flow devastated the community of Panabaj and was caused by heavy rainfall. During flow, segregation occurred with the coarse-grained fraction of sand, gravel and rocks coming to rest partly down slope, while the fine-grained portion of water and fine sediment (40% of the volume) continued to move in a less turbulent manner, see Figure 1.

Current research on granular flows ranges from idealized laboratory set-ups in which rather uniform dry granular matter is considered, to water-saturated poly-dispersed debris flows over complex terrain. Mono-dispersed irregular and spherical particles have been used by Denlinger and Iverson 2001 (dry sand), Gray et al. 2003 (non-pareille sugar grains or `sprinkles') Hákonardóttir and Hogg 2005 (almost spherical glass ballotini), Börzsönyi and Ecke 2007 (sand, glass and copper particles), and Vreman et al. 2007 (glass beads and poppy seeds) to study granular flows, whereas, bi-dispersed (in size) spherical particles were used to study segregation by Thornton et al. 2006. Denlinger and Iverson 2001 also investigated water-saturated sand and gravel, bringing the problem under consideration closer to real natural debris flows. We will distinguish broadly two modeling philosophies in the research on shallow granular flows: detailed modeling using idealized particle types and flow geometries, and more realistic

modeling with complex particle types over complex terrain.

Figure 1: The Panabaj debris flow displayed strong segregation into coarse- and fine-grained material such as sand, gravel and rock as seen from the remnants at higher elevations (coarser debris on the left); and, fine-grained water and fine-sediment constituents in the channel lower down the volcano (finer debris on the right). Photo courtesy: Laura Connor.[1]

The first modeling philosophy aims to verify and validate the shallow granular flow models accurately against experimental flow measurements for uniform particle sizes, shapes and densities in simple geometries. Often solutions from hydraulic theory are used, and these carry over to granular flows: hydraulic jumps/bores for shallow water flows become granular jumps and bores. A jump or bore is a discontinuity in the depth and velocity of the flow that propagates at a well-defined velocity. In granular flows this bore is localized over five-to-ten particle diameters, in sharp contrast to water flows where a longer turbulent and bubbly region around the broken wave is observed. Figure 2 compares a hydraulic and granular bore and illustrates the sharper transition in the granular case. For dilute granular flows, kinetic theory has validity (e.g.,

---

[1] Connor, C.N., Connor, L., Sheridan, M. 2006. Assessment of Oct. 2005 debris flows at Panabaj, Guatamala, and recommendations for hazard mitigation. For Oxfam G.B.

Jenkins 2006) and has been used to determine stress and constitutive laws for both mono- and bi-dispersed spherical particles: again strengthening granular flow research in idealized circumstances. In the second modeling philosophy, experiments use more realistic fluid-saturated particles with wide size distributions (Denlinger and Iverson 2001, 2004). Then, an averaged constitutive law is considered, and validation is done against shallow granular flow over complex terrain, such that the interactions between flow and terrain are the discriminating factors. While the second philosophy is more relevant for environmental applications, the first one allows closer comparisons between experimental data, theory and simulations. Of course, models used in the second philosophy should be reducible to ones used in the first philosophy. We will limit ourselves mainly to the first philosophy with its idealizations.[1]

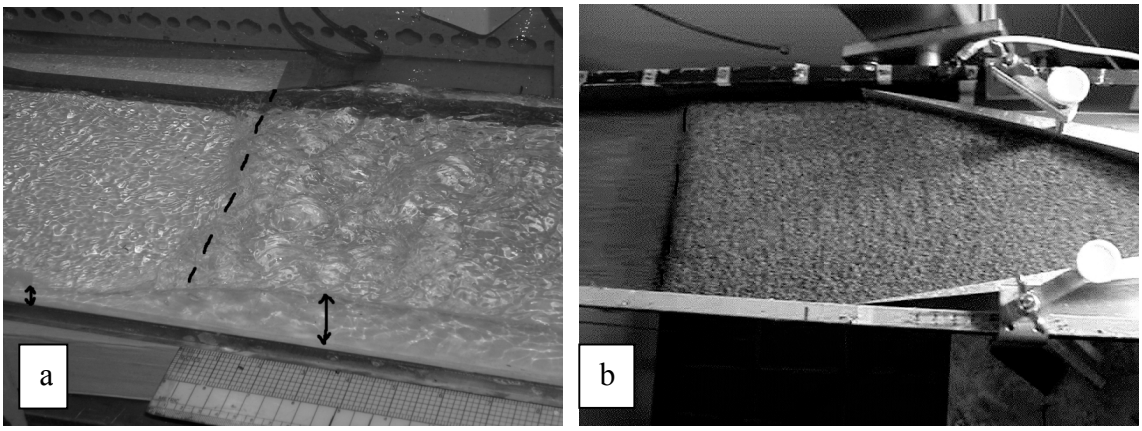

Figure 2: a) A hydraulic jump in a horizontal channel has steadied against the incoming fast flow from the left; photo courtesy: Benjamin Akers (University of Illinois -Chicago, U.S.A.). b) A granular bore on an inclined channel is moving upstream due to the contraction in the channel; the incoming fast flow of poppy seeds slows down after the jump. Bore fronts are indicated and in the hydraulic case also water heights. Flows are from left to right.

[1] See the chapter on debris flows by R.M. Iverson.

In the remainder of this chapter, we will start by deriving shallow depth-averaged granular flow equations in the absence of particle segregation, and the associated bore relations. Then we consider the validity of these equations for several basal stress relations for both smooth and rough topography (Section II). Our second goal is to analyze a model of particle segregation for bi-dispersed flows with an interstitial fluid and compare its predictions to chute flow experiments (Section III). In both cases, we discuss limitations and possible extensions to these models. Finally, we combine the two goals and outline future challenges in Section IV.

II. DEPTH-AVERAGED SHALLOW GRANULAR FLOW MODELS

Cauchy Balance Equations

In this section a model for shallow granular flow will be derived. The starting point will be Cauchy's equations for mass and momentum

$$\frac{D\rho}{Dt} + \rho\left(\nabla \cdot \underline{u}\right) = 0 \text{ and } \frac{D}{Dt}\left(\rho \underline{u}\right) = \nabla \cdot \underline{\underline{\sigma}} + \rho \underline{B} . \tag{1.1}$$

These conservation laws must be satisfied by all solids, liquids and gasses. In the above equations, the material density is ρ, velocity $\underline{u} = (u, v, w)^T$, the stress tensor is $\underline{\underline{\sigma}}$, and the external body force is $\underline{B}$. The material derivative $D/Dt = \partial/\partial t + \underline{u} \cdot \nabla$, with gradient ∇ and time t, is the rate of change in time taken along a path moving with a material element. To solve these equations a model for the stress tensor and the body forces is required. From conservation of angular momentum, it can be shown that the stress tensor must be symmetric and this means it has six independent components in three dimensions and only three in two dimensions.

Shallow Granular Flows

We will proceed by making a series of approximations to obtain a simpler set of equations for

shallow granular flows. This was first done by Savage and Hutter (1989)[1]; however, here we follow the derivation by Gray et al. (2003). The fluidized granular material is assumed to be incompressible and homogeneous with constant density ρ_0. It thus includes certain granular mixtures with particles of different densities, shapes and sizes, in the absence of segregation. The only external body force acting is gravity, and attention will be restricted to two-dimensional flows, as illustrated in Figure 3. Hence, system (1.1) reduces to the following system of partial differential equations for *u*, *w* and stress components σ_{xx}, σ_{xz} and σ_{zz}:

$$\frac{\partial u}{\partial x} + \frac{\partial w}{\partial z} = 0$$

$$\rho\left(\frac{\partial u}{\partial t} + \frac{\partial u^2}{\partial x} + \frac{\partial}{\partial z}(uw)\right) = \rho g \sin\theta + \frac{\partial \sigma_{xx}}{\partial x} + \frac{\partial \sigma_{xz}}{\partial z}, \qquad (1.2)$$

$$\rho\left(\frac{\partial w}{\partial t} + \frac{\partial}{\partial x}(uw) + \frac{\partial w^2}{\partial z}\right) = -\rho g \cos\theta + \frac{\partial \sigma_{xz}}{\partial x} + \frac{\partial \sigma_{zz}}{\partial z}$$

with g the acceleration of gravity and θ the inclination of the coordinate system (Figure 3).

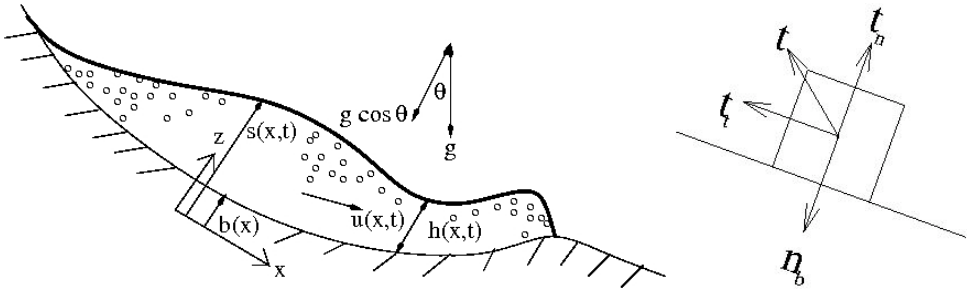

Figure 3: Sketches are given of the domain with coordinate z normal to and coordinate x along the inclined base with layer thickness $h(x,t) = s(x,t) - b(x)$, and (right sketch) the contact forces involved at the base.

[1] It should be noted that similar models appeared in the Russian literature in the 60/70's, but English translations are hard to obtain.

Boundary Conditions

As follows from Figure 3, the free and basal surfaces are described by $z - s(x,t) = 0$ and $b(x,t) - z = 0$, respectively, with coordinate z lying normal to an average slope. The **kinematic** boundary conditions must hold there, such that

$$\frac{D(s-z)}{Dt} = \frac{\partial s}{\partial t} + u^s \frac{\partial s}{\partial x} - w^s = 0 \text{ and } \frac{D(b-z)}{Dt} = \frac{\partial b}{\partial t} + u^b \frac{\partial b}{\partial x} - w^b = 0. \qquad (1.3)$$

Superscripts here denote evaluation at free and basal surfaces. The boundaries are impermeable, which for fixed boundaries reduces to the more familiar condition $\underline{u} \cdot \underline{n} = 0$ with outward normal $\underline{n}$ at the fixed boundary. We limit ourselves to one coordinate frame, and refer to the literature for extensions of the shallow layer equations in curvilinear coordinates (e.g., Denlinger and Iverson 2004). The latter is required for shallow flows over highly variable terrain.

The force per unit area applied to each of the boundaries (the traction) must be specified. Since the free surface is assumed to be open, it is traction-free (i.e., no force is applied), which means $\underline{\underline{\sigma}}^s \underline{n}^s = 0$. On the base a Coulomb friction model (for flowing material) will be implemented $\underline{t}_t = -\mu |\underline{t}_n| \underline{u} / |\underline{u}|$, stating that the tangential component of the traction is proportional to the normal component of the traction and acts in a direction opposing the motion. The proportionality factor μ can be a function of both the local depth and velocity of the flow. It should, however, be noted that this friction model is a limiting state, valid for flowing material, and care needs to be taken when considering material that is arresting or starts to flow. The traction on the base is given by $\underline{t}^b = \underline{\underline{\sigma}}^b \underline{n}^b$, which can be decomposed into normal and tangential components as follows: $\underline{t}^b = \underline{t}_t^b + \underline{t}_n^b = \underline{t}_t^b - \underline{n}^b |\underline{t}_n^b|$ (the minus sign indicates the normal forces act into the domain, see Figure 3). Now clearly $|\underline{t}_n^b| = -\underline{n}^b \cdot \underline{t}^b = -\underline{n}^b \cdot \left(\underline{\underline{\sigma}}^b \underline{n}^b\right)$, which implies

$$\underline{\underline{\sigma}}^b \underline{n}^b = \mu\left(\underline{n}^b \cdot \underline{\underline{\sigma}}^b \underline{n}^b\right)\frac{\underline{u}^b}{\left|\underline{u}^b\right|} + \left(\underline{n}^b \cdot \underline{\underline{\sigma}}^b \underline{n}^b\right)\underline{n}^b . \tag{1.4}$$

Finally, to apply these boundary conditions, the surface normal vectors $\underline{n}^b$ and $\underline{n}^s$ are expressed in terms of the unit normal vectors $\underline{e}_x$ and $\underline{e}_z$. From the basic geometry, see Figure 3, it is clear that $\Delta^s \underline{n}^s = -\left(\partial s / \partial x\right)\underline{e}_x + \underline{e}_z$, and $\Delta^b \underline{n}^b = \left(\partial b / \partial x\right)\underline{e}_x - \underline{e}_z$ where the normalization factors Δ^ν are given by $\Delta^\nu = \sqrt{\left(\partial \nu / \partial x\right)^2 + 1}$ for $\nu = s,b$.

Dimensionless form

We proceed by writing the equations in dimensionless form. This results in the appearance of a dimensionless aspect ratio ε and its smallness will be employed later to simplify the equations.

Let L be a typical flow length, H a typical flow depth with g the magnitude of the gravitational acceleration. Then the following dimensionless variables are introduced

$$x = L\tilde{x},\ z = H\tilde{z},\ t = \sqrt{L/g}\,\tilde{t},\ u = \sqrt{Lg}\,\tilde{u},\ w = \varepsilon\sqrt{Lg}\,\tilde{w},$$

$$\sigma_{xx} = \rho_0 g H \tilde{\sigma}_{xx}, \sigma_{zz} = \rho_0 g H \tilde{\sigma}_{zz} \text{ and } \sigma_{xz} = \varepsilon^\gamma \rho_0 g H \tilde{\sigma}_{xz},$$

where $\varepsilon = H / L$ and $0 < \gamma < 1$. Applying this scaling to the governing equations (1.2) yields,

$$\frac{\partial \tilde{u}}{\partial \tilde{x}} + \frac{\partial \tilde{w}}{\partial \tilde{z}} = 0, \tag{1.5}$$

$$\frac{\partial \tilde{u}}{\partial \tilde{t}} + \frac{\partial \tilde{u}^2}{\partial \tilde{x}} + \frac{\partial}{\partial \tilde{z}}\left(\tilde{u}\tilde{w}\right) = \sin\theta + \varepsilon\frac{\partial \tilde{\sigma}_{xx}}{\partial \tilde{x}} + \varepsilon^\gamma \frac{\partial(\tilde{\sigma}_{xz})}{\partial \tilde{z}} \text{ and} \tag{1.6}$$

$$\varepsilon\left(\frac{\partial \tilde{w}}{\partial \tilde{t}} + \frac{\partial}{\partial \tilde{x}}\left(\tilde{u}\tilde{w}\right) + \frac{\partial \tilde{w}^2}{\partial \tilde{z}}\right) = -\cos\theta + \varepsilon^{1+\gamma}\frac{\partial(\tilde{\sigma}_{xz})}{\partial \tilde{x}} + \frac{\partial \tilde{\sigma}_{zz}}{\partial \tilde{z}}, \tag{1.7}$$

Similarly, applying the scaling to boundary equations (1.3) and (1.4) leads to the following conditions at the free surface

$$\frac{\partial \tilde{s}}{\partial \tilde{t}} + \tilde{u}^s \frac{\partial \tilde{s}}{\partial \tilde{x}} - \tilde{w}^s = 0,\ -\varepsilon \sigma^s_{xx} \frac{\partial s}{\partial x} + \varepsilon^\gamma \sigma^s_{xz} = 0 \text{ and } -\varepsilon^{1+\gamma} \sigma^s_{xz} \frac{\partial s}{\partial x} + \sigma^s_{zz} = 0, \tag{1.8}$$

and at the basal surface

$$\begin{gathered} \frac{\partial \tilde{b}}{\partial \tilde{t}} + \tilde{u}^b \frac{\partial \tilde{b}}{\partial \tilde{x}} - \tilde{w}^b = 0 \ ,\ \varepsilon \tilde{\sigma}^b_{xx} \frac{\partial \tilde{b}}{\partial \tilde{x}} - \varepsilon^\gamma \tilde{\sigma}^b_{xz} = \left(\underline{\tilde{n}}^b \bullet \underline{\underline{\tilde{\sigma}}}^b \underline{\tilde{n}}^b \right) \left(\tilde{\Delta}^b \left(\tilde{u}^b \,/\, \left| \underline{\tilde{u}}^b \right| \right) \mu + \varepsilon \frac{\partial \tilde{b}}{\partial \tilde{x}} \right) \\ \text{and} \quad \varepsilon^{\gamma+1} \tilde{\sigma}^b_{xz} \frac{\partial \tilde{b}}{\partial \tilde{x}} - \tilde{\sigma}^b_{zz} = \left(\underline{\tilde{n}}^b \bullet \underline{\underline{\tilde{\sigma}}}^b \underline{\tilde{n}}^b \right) \left(\tilde{\Delta}^b \left(\varepsilon \tilde{w} \,/\, \left| \underline{\tilde{u}} \right| \right) \mu - 1 \right). \end{gathered} \tag{1.9}$$

Depth averaged modeling

The main idea of depth averaging is to integrate out the *z*-dependence (recall that *z* is the spatial coordinate normal to the base). This process results in a model of lower dimension, yet it is not equivalent to setting the *z*-derivative to zero since velocity component *w* remains dependent on *z*. The height or depth of the flow in the z-direction is defined as $h = s - b$. The depth-averaged value $\bar{f}$ of a variable *f* is given by $\bar{f} = (1/h)\int_b^s f dz$. Integration of (1.5) over depth while using kinematic conditions (1.8) and (1.9) yields, after dropping the tildes,

$$\frac{\partial h}{\partial t} + \frac{\partial}{\partial x}\left(h\bar{u} \right) = 0. \tag{1.10}$$

Depth averaging the *x*-momentum equation (1.6), in the same manner yields

$$\frac{\partial}{\partial t}\left(h\bar{u} \right) + \frac{\partial h\overline{u^2}}{\partial x} - \left[u\left(\frac{\partial z}{\partial t} + u\frac{\partial z}{\partial x} - w \right) \right]_b^s = h\sin\theta + \varepsilon \frac{\partial}{\partial x}\left(h\bar{\sigma}_{xx} \right) - \left[\varepsilon \sigma_{xx} \frac{\partial z}{\partial x} - \varepsilon^\gamma \sigma_{xz} \right]_b^s. \tag{1.11}$$

Using the kinematic and traction boundary conditions (1.8) and (1.9), the terms in the square brackets of (1.11) can be simplified to give

$$\frac{\partial}{\partial t}\left(h\bar{u} \right) + \frac{\partial h\overline{u^2}}{\partial x} = h\sin\theta + \varepsilon \frac{\partial}{\partial x}\left(h\bar{\sigma}_{xx} \right) + \left(\mu \Delta^b \frac{\bar{u}^b}{\left| \underline{\bar{u}}^b \right|} + \varepsilon \frac{\partial b}{\partial x} \right) \left(\underline{n}^b \bullet \underline{\underline{\sigma}}^b \underline{n}^b \right). \tag{1.12}$$

Exercise 1: Verify derivations (1.10) and (1.12). Employ Leibniz' rule and use $\bar{u} = u^b + O(\varepsilon)$.

Order of magnitude estimates

As discussed in detail in previous sections, granular flows are often long and shallow and so far we have not exploited this fact; mathematically this implies that $\varepsilon = H / L \ll 1$. In the following treatment terms of order greater than ε will be neglected and the order of the tangential stress must be discussed. If it is assumed that $0 < \gamma < 1$, then only leading order terms in the scalar factor $\left(\underline{n}^b \bullet \underline{\underline{\sigma}}^b \underline{n}^b\right)$ need to be retained. Expansion gives $\left(\underline{n}^b \bullet \underline{\underline{\sigma}}^b \underline{n}^b\right) = \sigma_{zz}\big|_b + O(\varepsilon)$. From (1.7) the leading order behavior of σ_{zz} is governed by the solution of $\partial\sigma_{zz} / \partial z = \cos\theta$, whose integration (using (1.8) at leading order such that $\sigma^s_{zz} = 0$) gives

$$\sigma_{zz} = (z - s)\cos\theta + O(\varepsilon). \tag{1.13}$$

Hence, $\sigma_{zz}\big|_b = -h\cos\theta + O(\varepsilon)$ and by retaining terms to $O(\varepsilon)$, equation (1.12) is rewritten as

$$\frac{\partial}{\partial t}(h\bar{u}) + \frac{\partial}{\partial x}\left(h\overline{u^2}\right) = h(\sin\theta - \mu\cos\theta\frac{\bar{u}}{|\bar{u}|}) + \varepsilon\frac{\partial}{\partial x}\left(h\bar{\sigma}_{xx}\right) - \varepsilon h\cos\theta\frac{\partial b}{\partial x} + O\left(\varepsilon^{1+\gamma}\right), \tag{1.14}$$

since in one dimension $|\underline{\bar{u}}| = \sqrt{\bar{u}^2 + \varepsilon^2\bar{w}^2} \approx |\bar{u}|$ and $\Delta^b \approx 1$. To close the model a constitutive relation for $\bar{\sigma}_{xx}$, a model for μ and the depth -averaged square velocity $\overline{u^2}$ need to be specified. These closures are still open research questions and will be discussed in more detail below.

Constitutive model for $\bar{\sigma}_{xx}$ and depth-integrated square velocity

In the original paper of Savage and Hutter (1989) they assumed the granular material behaved as a Mohr-Coulomb material in yield, which gives $\sigma_{xx} = K\sigma_{zz}$. The material constant K is called the Earth pressure coefficient and is given by

$$K = 2\sec^2\phi_i\left(1 \mp \left(1 - \cos^2\phi_i\sec^2\phi\right)^{1/2}\right) - 1, \tag{1.15}$$

where ϕ_i is the internal angle of friction and ϕ is the basal friction angle. The minus sign is taken for material in an active state, i.e. $\partial\bar{u}/\partial x > 0$, and the positive sign for material in a passive state, i.e. $\partial\bar{u}/\partial x < 0$ (see also Iverson and Denlinger 2001). A simpler model is to assume a flowing granular material acts like an inviscid fluid, implying $K = 1$. We will retain K and leave its choice to the reader. Finally, from $\sigma_{xx} = K\sigma_{zz}$ and (1.13) it follows that

$$\bar{\sigma}_{xx} = -Kh\cos\theta/2. \tag{1.16}$$

Using $h\int_b^s u^2 dz = \alpha_1\left(\int_b^s u dz\right)^2$, the depth-average square velocity can be expressed in terms of the squared depth-average velocity as follows:

$$\overline{u^2} = \alpha_1\bar{u}^2. \tag{1.17}$$

The shape-factor α_1 gives information about the vertical velocity profile. For a parabolic velocity profile (with zero basal velocity) $\alpha_1 = 6/5$, and for realistic nearly uniform velocity profiles $\alpha_1 \approx 1$ (e.g., GDR Midi 2004). The latter will be assumed here.

The shallow layer equations and granular jumps or shocks

Substitution of (1.16) and (1.17) into (1.14) leads together with (1.10) to shallow layer equations

$$\begin{gathered}\frac{\partial h}{\partial t} + \frac{\partial}{\partial x}(hu) = 0 \\ \frac{\partial}{\partial t}(hu) + \frac{\partial}{\partial x}(hu^2) + \varepsilon K\cos\theta\frac{\partial}{\partial x}\left(\frac{h^2}{2}\right) = h(\sin\theta - \mu\frac{u}{|u|}\cos\theta) - \varepsilon h\cos\theta\frac{\partial b}{\partial x}\end{gathered}, \tag{1.18}$$

where basal friction $\mu = \tan\phi$ with basal friction angle ϕ. Bars and higher order terms in ε have been dropped. The basal friction μ and hence ϕ, in general, depend on the flow variables h and u, as will be discussed in detail later. The system of equations (1.18) is hyperbolic and hence discontinuous (shock) solutions are possible. In the hydraulic literature, these discontinuous

solutions are generally called hydraulic jumps or bores instead of shocks as is usual in gas dynamics. The differential (strong) form implies implicitly that both *h* and *u* are continuous; therefore, to obtain shock relations we must use the integral (weak) form. Here, the weak form and associated shock relation will be derived for the mass balance equation, whereas similar results for the momentum balance will be left as an exercise.

First, we integrate the depth-average mass balance equations (1.18) from $X(t)-\delta$ to $X(t)+\delta$ and take the limit $\delta \to 0$, with both *h* and *u* discontinuous at $x = X(t)$. Defining X^- as the limit position on the left side of the jump and X^+ the limit on the right side, and bore speed $S = dX/dt$, this integral equation becomes $\frac{d}{dt}\int_{X^-(t)}^{X^+(t)} h\,dx - S[h]_{X^-}^{X^+} + [hu]_{X^-}^{X^+} = 0$, after applying Leibniz's rule. Of course, the term $\int_{X^-(t)}^{X^+(t)} h\,dx = 0$. Altogether, we obtain the jump relation for the continuity equations and similarly the one for the momentum equation:

$$\left[h(u-S)\right]_-^+ = 0 \text{ and } \left[hu(u-S)\right] = -\left[\varepsilon K h^2 \cos\theta/2\right]_-^+, \tag{1.19}$$

where the +/- subscripts indicate the states on the right/left of the shock.

Exercise 2: Derive the above bore/shock relation (1.19) for the momentum equation.

By analogy with (1.18), the two-dimensional shallow layer equations are

$$\begin{aligned}
&\frac{\partial h}{\partial t} + \frac{\partial}{\partial x}(hu) + \frac{\partial}{\partial y}(hv) = 0 \\
&\frac{\partial}{\partial t}(hu) + \frac{\partial}{\partial x}\left(hu^2 + \varepsilon K\cos\theta\frac{h^2}{2}\right) + \frac{\partial}{\partial y}(huv) = h(\sin\theta - \mu\frac{u}{|\underline{u}|}\cos\theta) - \varepsilon h\cos\theta\frac{\partial b}{\partial x} \\
&\frac{\partial}{\partial t}(hv) + \frac{\partial}{\partial x}(huv) + \frac{\partial}{\partial y}\left(hv^2 + \varepsilon K\cos\theta\frac{h^2}{2}\right) = -\mu\frac{hv}{|\underline{u}|}\cos\theta - \varepsilon h\cos\theta\frac{\partial b}{\partial y}
\end{aligned} \tag{1.20}$$

with velocity v in the y–direction. The following shock relations arise from (1.20):

$$\left[h\left(\underline{u}\cdot\underline{n}-S\right)\right]_{-}^{+}=0 \text{ and } \left[h\underline{u}\left(\underline{u}\cdot\underline{n}-S\right)\right]_{-}^{+}+\left[\varepsilon Kh^{2}\cos\theta/2\right]_{-}^{+}\underline{n}=0, \tag{1.21}$$

where we defined the unit vector $\underline{n}$ normal to the bore in the direction of the drop in depth; S is the bore speed in that direction.

Exercise 3: Derive the shallow granular layer equations (1.20) by extending the derivation given for the one-dimensional case to the two-dimensional case, cf. Gray et al. (2003), for the simplified case with $K=1$ such that $\sigma_{xx}=\sigma_{yy}=\sigma_{zz}$.

Exercise 4: Similarly derive the bore relations (1.21) corresponding to the two-dimensional shallow layer equations (1.20).

Applications

Several studies have compared solutions of the shallow layer equations in one- and two-dimensions over inclined topography, or extensions thereof, against data of laboratory or field experiments. The particulate matter used in these studies involved a range of materials, such as relatively uniform sugar grains, sand or copper particles; nearly spherical glass beads in small diameter ranges; and, poppy and mustard seeds, among others. The surface of the topography varied from smooth (wood or aluminum) to rough (sand paper, velvet, or particles glued onto the surface). We will consider several idealized results with uniform particles and specific geometries, and the corresponding choices of K and μ.

Starting with studies on smooth chutes, Gray et al. (2003) compared numerical simulations of (1.20) by using $K=1$ with laboratory experiments on non-accelerating slopes. Forcing and basal friction were therefore in balance with $\mu=\tan\phi=\tan\theta$. Nearly one-dimensional granular bores were generated by entirely blocking the chute. We follow Vreman et al. (2007), who also included the solid fraction $\alpha_{\pm}$ before and after the bore. The bore speed in this one-dimensional case becomes

$$S = -\sqrt{\frac{1}{2}\varepsilon K \cos\theta(\alpha_- h_- / \alpha_+ h_+)(\alpha_+ h_+^2 - \alpha_- h_-^2)/(\alpha_+ h_+ - \alpha_- h_-)}, \qquad (1.22)$$

with constant inflow speed u_-, depth h_- and solid fraction α_-. For dilute inflows, Vreman et al. (2007) showed that including the difference in solid fraction, e.g., $\alpha_- = 0.36 \pm 0.06$ and $\alpha_+ \approx 0.64$, before and after the bore passes, yields a more accurate bore speed. The comparisons between numerical simulations of their shallow flow model in two dimensions and experiments of granular flow around a pyramid obstacle placed in the middle of the flow in Gray et al. (2003) were quite successful. These predictions included transient flow with particle-free regions and dead zones, where the particles are motionless.

Exercise 5: Derive the bore speed (1.22) for the case with the solid's volume fraction α constant, and roughly equal to the random packing fraction. To compute the bore speed what information must be the known or measured, also for the case with variable α?

Hákonardóttir and Hogg (2005) considered oblique shocks in rapid granular flows more extensively than Gray et al (2003). They also took $K = 1$ and $\mu = \tan\phi = \tan\theta$ and a relatively smooth, wooden inclined chute was used. A key parameter in these flows is the Froude number $F = u/\sqrt{\varepsilon \cos\theta K h}$, i.e., the ratio of fluid velocity u over the speed $\sqrt{\varepsilon K h \cos\theta}$ of granular free-surface gravity waves. In dimensional form this speed is $\sqrt{g \cos\theta K h}$ and $F = u/\sqrt{g \cos\theta K h}$.

Flows with Froude number greater than one are called supercritical, whereas other flows are termed subcritical. This is akin to the demarcation of compressible flows into sub- and supersonic flows based on the Mach number, the ratio of the flow speed over the speed of sound. Hákonardóttir and Hogg (2005) investigate supercritical flows with inflow numbers $F > 4$ against a straight barrier with a deflection angle θ_c with respect to a half-channel wall. For certain sufficiently supercritical flows, steady oblique hydraulic jumps with shock speed $S = 0$

emerge with an angle $\theta_s > \theta_c$ to the wall. The expressions follow from (1.21) as

$$2F_-^2 \sin^2\theta_s = \frac{1}{h_-}\frac{\alpha_+ h_+}{\alpha_- h_-}\frac{(\alpha_- h_-^2 - \alpha_+ h_+^2)}{(\alpha_- h_- - \alpha_+ h_+)} \text{ and } \frac{\alpha_+ h_+}{\alpha_- h_-} = \frac{\tan\theta_s}{\tan(\theta_s - \theta_c)}, \tag{1.23}$$

where F_- is the Froude number of the incoming flow. Again, we have included the solid's volume fraction α. Very good agreement was found between theory and experiment for constant α, while for dilute inflows the inclusion of different solid fractions remains important.

Exercise 6 (harder): Derive (1.23) from (1.21) by considering the momentum component along and orthogonal to the bore "propagation" direction. First draw a defining sketch of the situation, including the unit vectors normal and tangential to the granular jump.

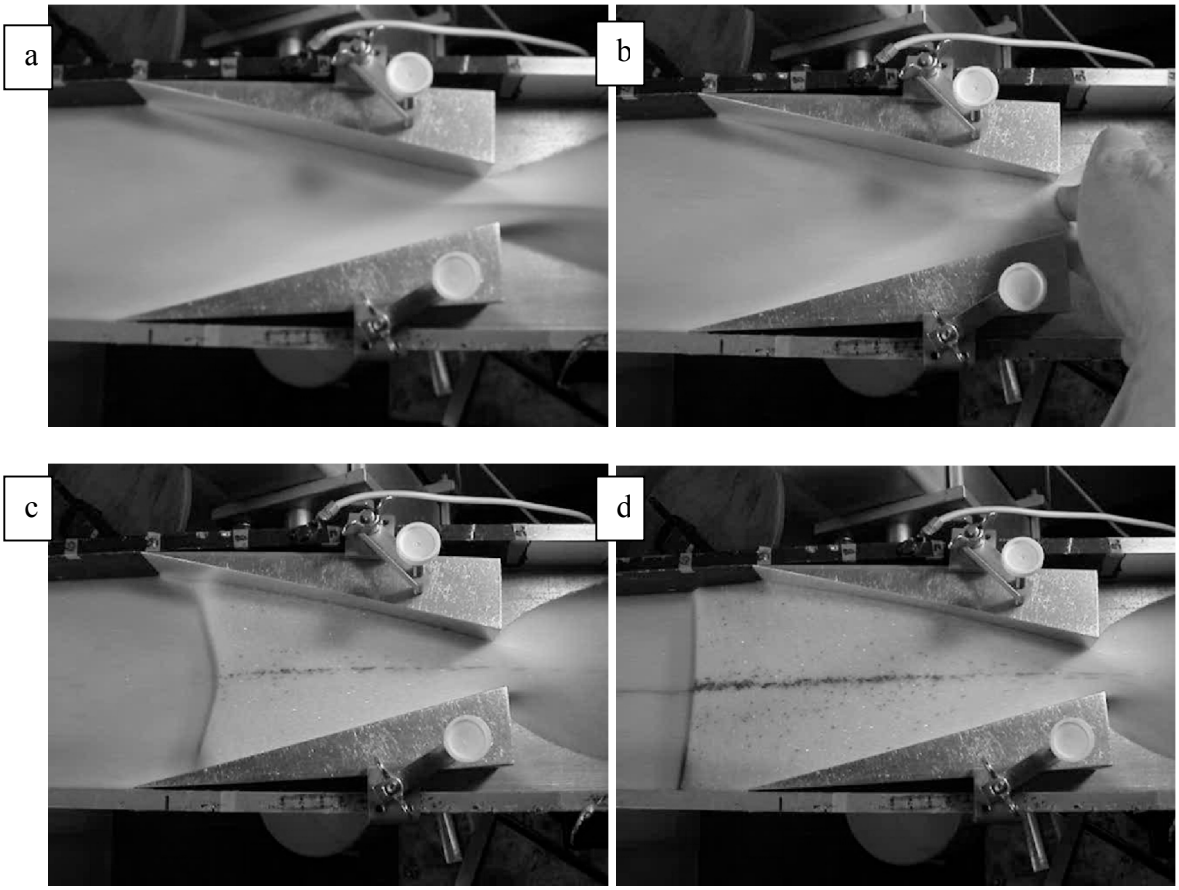

Figure 4: We view the contraction normal to the inclined chute. Panel (a) shows the smooth granular flow of glass beads with two weak oblique jumps. When we manually disturb this flow

by partially blocking the contraction exit for a short time, panel (b), the smooth flow state I in (a) changes to the reservoir state III with a clear granular jump in (c) and upstream bore state II in (d). This transition is displayed in the plates going from top left to bottom right. The top left plate manifests flow with smooth oblique jumps and the bottom right plate flow with an upstream halted jump and lake. All cases clearly show a jet behind the contraction. Inflow conditions at the left, upstream side are constant. Stray poppy seeds play the role of markers. ©J. Fluid Mech.

Inspired by lake formation in the Rhine River due to ash flows after the Laacher See volcanic eruption 12.900aBP and research in hydraulics, Vreman et al. (2007) considered supercritical granular flow on a smooth aluminum incline through a linear and localized contraction, see Figure 4 for a series of snapshots. The linear contraction consisted of two equal triangular aluminum blocks snug tightly to the channel walls. Glass beads in several diameter ranges and poppy seeds were used. While the incoming flows were always supercritical, the contraction allowed the emergence of several steady states including ones with a transition to subcritical flows. Two parameters govern the flow: upstream Froude number $F = u / \sqrt{g \cos\theta K h}$ and scaled minimum contraction width $0 \le B_c = b_c / b_- \le 1$ with constant upstream channel width b_-. Without the contraction $B_c = 1$, the chute inclination θ was adjusted such that the flow was steady and uniform (far enough away from the upstream inflow sluice gate). In this case we can take $\mu = \tan\phi = \tan\theta$ and also $K = 1$. In the presence of the contraction, several steady sometimes coexisting states can emerge. When the contraction width is relatively large, including $B_c \sim 1$, two oblique jumps emerge from the contraction walls and potentially collide in the middle of the contraction to form two new oblique jumps, et cetera. This state I is relatively smooth because the jumps are weak, see Figure 4.a. After the contraction, a free jet flows downstream. When the contraction is sufficiently closed, including $B_c \sim 0$, then it acts as a block

and an upstream moving granular bore emerges traveling towards the upstream sluice gate. This is state II, as seen in Figure 4.d. For intermediate values of the contraction width, regions emerge where the various states coexist, including a reservoir state III with a complex pattern of jumps in the contraction, see Figure 4.c. Note that the Froude number becomes subcritical behind the hydraulic jump for the state with the upstream moving bore and the reservoir state. While for the supercritical inflows, and also for the state with the weak oblique jumps, the Froude number stays nearly constant such that the forcing due to gravity and the friction due to inter-particle and particle-wall collisions are (nearly) in balance, with $\mu(F>1)=\tan\phi\approx\tan\theta$, the Coulomb friction factor is seen to decrease for the subcritical case such that $\mu(F<1)=\tan\phi<\tan\theta$. From (1.18) or (1.20), we thus see that the flow effectively accelerates in subcritical regions, relative to supercritical flow regions. In Figure 5, a comparison between the laboratory experiments and the one-dimensional hydraulic model is made using adjustable parameters Z_1 and Z_2, which are related to $\mu(F>1)$ and $\mu(F<1)$. When forcing and friction are in balance, parameter Z_1 is zero and $\mu=\tan\phi=\tan\theta$. The curves shown emerge from analytical expressions, which are extensions of classical hydraulic theory for a width average of the two-dimensional equations (1.20). These width-averaged equations are simplified in a similar manner as the depth-averaged case. Unfortunately, Vreman et al. (2007) could not further constrain the dependence of μ on, e.g., F and h. This result is important because it reveals that, although fixing μ may be valid for certain supercritical granular flows, it is not for subcritical flows. Further comparison (Vreman et al. 2007) between DPMs, in which all particles were simulated microscopically and stress relations were analyzed, revealed the shortcomings of several shallow layer equations used in the literature. This comparison was an a priori analysis because shallow layer models were not analyzed and validated, but only their specific stress relations.

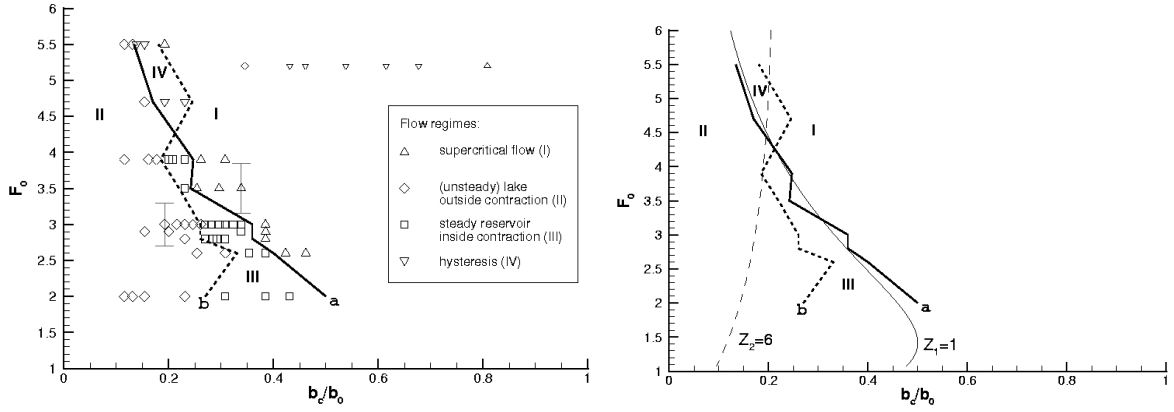

Figure 5: Left: Experimental granular results collected in a phase diagram spanned by Froude number versus nozzle width. Flow regimes observed are: (I) smooth supercritical flows, (II) steady lakes halting outside the contraction or upstream moving bore, (III) steady reservoirs with a granular or hydraulic jump inside the contraction, and (IV) a hysteretic region with multiple flow states (Figure 4). Drawn solid and dashed lines demarcate transitions between (a) regimes IV-I and II-III, and (b) II-IV and III-I. Representative error bars are shown. Tiny symbols (upper right corner) denote poppy seed experiments falling outside our classification. Right: comparison between analytical and experimental demarcation lines. ©J. Fluid Mech.

Kerswell (2005) investigated granular dam break or slumping problems with Coulomb friction on a horizontal surface. One-dimensional equations (1.18) were used with $b = 0$, $\theta = 0$ and constant $\mu = \tan\phi$. Corresponding analytical solutions were compared with a series of experimental data from the literature on both smooth and rough surfaces. Essentially, K, g and $\mu = \tan\phi$ could be combined into one fitting parameter after suitable rescaling. Such a recombination was argued to lead to a convenient (simplest) model to study granular slumping.

In contrast, steady flows on rough inclined chutes have been studied extensively (Pouliquen and Forterre 2002, GDR MIDI 2004, Börzsönyi and Ecke 2007) and reveal that

$\mu = \tan\phi$ depends on the (dimensional) Froude number $F = u/\sqrt{gh\cos\theta}$ and the depth h, as well as material fitting parameters. For relatively uniform sand grains, copper particles and glass beads the constitutive model determining μ was shown to follow the Pouliquen-Jenkins law. This was theoretically formulated by Jenkins (2006) using a phenomenological modification of granular kinetic theory to account for enduring particle contacts, revealing a slight modification to the law previously experimentally obtained by Pouliquen. The idea is that enduring contacts between grains, forced by the shearing (gradient of the particle velocity), reduce the collision rate of dissipation. Therefore a modification to the dissipation is introduced, which does not affect the stress. This (dimensional) Pouliquen-Jenkins law for flowing material reads

$$F_c = u/\sqrt{gh} = \beta(h/h_s)\tan^2\phi/\tan^2\phi_1, \tag{1.24}$$

with slope β as material parameter and the thickness

$$h_s(\phi) = Ad(\tan\phi_2 - \tan\phi)/(\tan\phi - \tan\phi_1), \text{ with } \phi_1 < \phi < \phi_2, \tag{1.25}$$

of the layer when the flow subsides, with particle diameter d and coefficient A. Hence, we must have $h \geq h_s$, which places a restriction on (1.24). The angles ϕ_1 and ϕ_2 are the angles where h_s diverges and approaches zero, respectively. Börzsönyi and Ecke (2007) confirmed this law against data from their laboratory experiments measured in the middle of the channel where wall effects are minimal. For steady uniform flow, the one-dimensional balance follows from (1.18) as: $\mu = \tan\phi = \tan\theta$ with a corresponding depth and velocity. Substitution of $\mu = \tan\phi$ and $\vartheta = uAd/(\beta h\sqrt{gh})$ in the above two expressions (1.24) and (1.25) and elimination of h_s yields the cubic equation

$$\mu^3 - \mu^2\tan\phi_1 + \mu\vartheta\tan^2\phi_1 - \vartheta\tan^2\phi_1\tan\phi_2 = 0. \tag{1.26}$$

Through division by $\tan^2\phi_1$ and use of $\tilde{\mu} = \mu/\tan\phi_1$ and $\eta = \tan\phi_2/\tan\phi_1$, we rewrite this cubic

equation as $\tilde{\mu}^3 - \tilde{\mu}^2 + \tilde{\mu}\vartheta - \vartheta\eta = 0$. It has only one real solution since $\eta > 1$ and the discriminant of this equation is negative. Given material parameters and the flow state combined into ϑ, this variable friction $\mu = \tan\phi$ can be determined and used in the equations of motion.

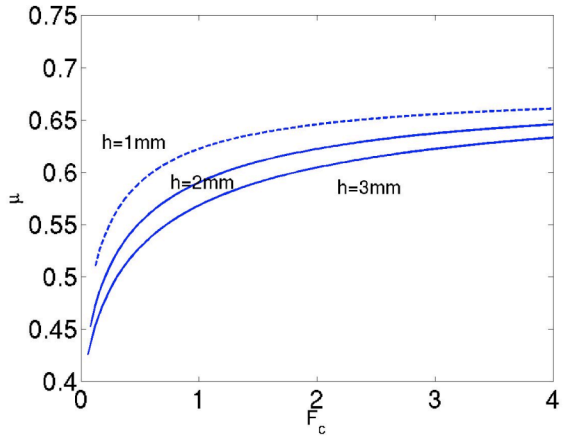

Figure 6: Basal friction versus Froude number $F_c = F\sqrt{\cos\theta} = u/\sqrt{gh}$ for glass beads (Börzsönyi and Ecke 2007): $A = 0.95$, $d = 0.72mm$, $\phi_1 = 20.8^o$,$\phi_2 = 34.2^o$, and $\beta = 0.06$.

This first version of the friction law (1.24) was obtained from experiments by allowing a flowing layer to become stationary and measuring $h_s(\phi)$. For most granular materials a greater angle is required to start stationary than to retard flowing material. By starting with a stationary layer and measuring the angle required to start motion Pouliquen and Forterre (2002) measured $h_{start}(\phi)$. They extended the friction law (1.24) to include this effect, allowing the study of problems with emerging and disappearing dead zones. We have plotted μ versus the Froude number in Figure 6 and it shows that the basal friction decreases with decreasing Froude number, similar to the Froude number dependence in the granular flow experiments in Vreman et al. (2007) on a smooth chute. How relevant these detailed studies of granular flows are under idealized conditions for (dry) granular particle flows in the field, such as landslides and pyroclastic flows, is an important question, which will be discussed in section IV.

III. PARTICLE SEGREGATION

The shallow granular model presented in section II assumes all the flow is either comprised of identical mono-dispersed particles or does not segregate for poly-dispersed ones, but this is far from reality. As discussed in the introduction, real geological flows are poly-dispersed and contain particles of different shape, roughness, size and density. In the high solid fraction regions of these flows the large particles commonly segregate to the surface, where they are transported to the margins to form bouldery flow fronts (see Figure 2 and the associated discussion in the introduction). In many natural flows these bouldery margins experience a much greater frictional force, leading to frontal instabilities (Iverson 1997). These instabilities create levees that channel the flow, thus vastly increasing the run-out distance. Gaining in-depth understanding of this effect is one of the major challenges in improving the predictive power of shallow granular models.

A similar effect can be observed in dry granular experiments with a combination of small smooth and large rough particles. When this mixture is poured down an inclined plane, particle size segregation causes large particles to accumulate near the margins. Being rougher, the large particles experience a greater frictional force and this configuration (rougher material in front of smoother) can be unstable (see Figure 7). This instability causes the uniform flow front to break up into a series of fingers (Pouliquen and Vallance 1999).

There are many mechanisms of segregation of dissimilar grains in granular materials (Cooke et al. 1976), but kinetic sieving is the mechanism that normally dominates in the dense granular flow regime where shallow granular avalanche models are applicable. The basic idea is that as grains avalanche down the slope, the local void ratio fluctuates, and the small particles fall into gaps that open up beneath them because they are simply more likely to fit into the

available space than the large ones. The small particles, therefore, migrate towards the bottom of the flow and lever the large particles upwards by force imbalances.

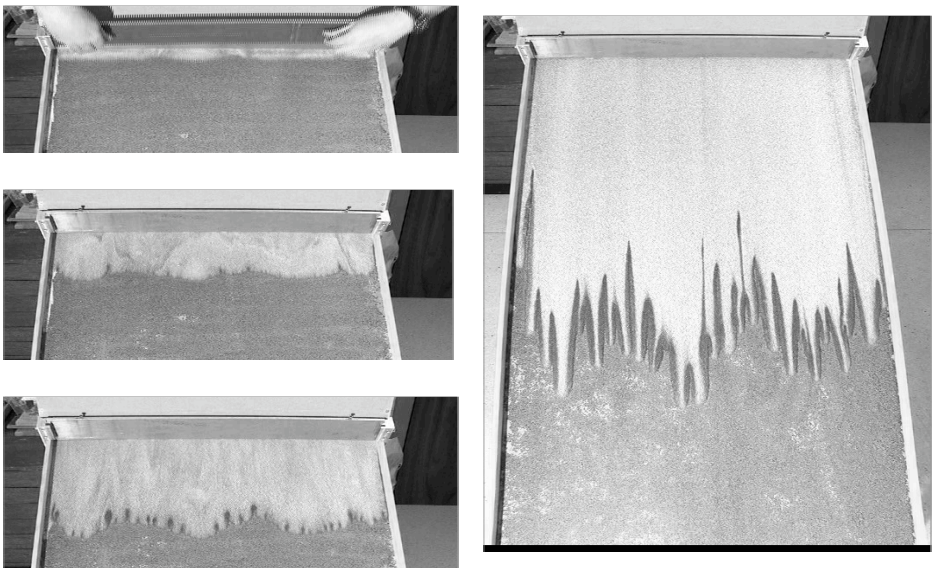

Figure 7: Four images show the fingering instability created by particle segregation at $t = 0,1.5,3,14s$. The chute measures $1 \times 2m^2$. The experiment is performed with a mixture of 17% black rough carborundum (315-355 μm) and 83% glass ballotini (75-150 μm). Courtesy: Nico Gray (University of Manchester, U.K.) and Pete Kokelaar (University of Liverpool, U.K.).

The first model of kinetic sieving was developed by Savage and Lun (1988), using a statistical argument about the distribution of void space. This model was able to predict steady-state size distributions for simple shear flows with bi-disperse granular materials. Recently, Thornton et al. (2006) developed the same structure from the framework of mixture theory. The two assumptions of this model are: firstly, as the different particles percolate past each other there is a Darcy-style drag between the different constituents (i.e. the small and large particles) and, secondly, particles falling into void spaces do not support any of the bed weight. Since the number of voids available for small particles to fall into is greater than for large particles, it

follows that a higher percentage of the small particles will be falling and, hence, not supporting any of the bed load.

Mixture theory assumes that all constituents, ν, simultaneously occupy every point in the material, with a local volume fraction Φ^ν. Then overlapping partial densities, ρ^ν, partial velocities, $\underline{u}^\nu$, and partial pressures, p^ν, can be defined for each constituent. These partial quantities can be related to their intrinsic (laboratory measured) value via the following relationships, $\rho^\nu = \Phi^\nu \rho^{\nu *}$, $p^\nu = f^\nu p$ and $\underline{u}^\nu = \underline{u}^{\nu *}$, where functions f^ν are to be determined and superscripts * indicate intrinsic variables. This formulation is very powerful as the following simple relationships hold for the bulk density, $\rho = \sum_\nu \rho^\nu$ and bulk pressure $p = \sum_\nu p^\nu$. Each of these constituents must satisfy individual mass and momentum balances

$$\frac{\partial \rho^\nu}{\partial t} + \nabla \cdot \left(\rho^\nu \underline{u}^\nu \right) = 0, \quad \frac{D^\nu}{D^\nu t} \left(\rho^\nu \underline{u}^\nu \right) = -\nabla p^\nu + \rho^\nu \underline{g} + \underline{\beta}^\nu , \tag{1.27}$$

where $\underline{\beta}^\nu$ is the interaction force exerted on phases ν by the other constituents. By definition the sum across all constituents of the $\underline{\beta}^\nu$'s must be zero. For simplicity, we will consider a two-constituent mixture theory (large, l, and small, s, particles), in which the interstitial pore space is incorporated into the volume of the grain, i.e. $\Phi^l + \Phi^s = 1$.

Exercise 7: Assume that large and small particles have the same intrinsic density $\rho^{s*} = \rho^{l*} = \rho_0$ and Dw/Dt is small, then show from vertical momentum balance that the bulk pressure is $p = \rho_0 g (h - z) \cos\theta$, with h the depth of the flow and θ the angle the flow makes to gravity.

To close this model we must specify the interaction force between large and small particles, and the pressure functions f^ν. Experiments show that the kinetic sieving process is similar to the percolation of fluids through a porous solid, and we therefore use a Darcy-style law

$$\underline{\beta}^{\nu} = p\nabla\cdot f^{\nu} - \rho^{\nu} c\left(\underline{u}^{\nu} - \underline{u}\right), \qquad \nu = l,s \quad . \tag{1.28}$$

The material constant c is the inter-particle drag coefficient and will in general depend on both species' surface properties, whereas $\underline{u} = \left(\rho^{l}\underline{u}^{l} + \rho^{s}\underline{u}^{s}\right)/\rho$ is the bulk velocity.

Exercise 8: Assuming that vertical accelerations are small, show that drag relation (1.28) implies

$$\Phi^{\nu} w^{\nu} = \Phi^{\nu} w + \left(f^{\nu} - \Phi^{\nu}\right)(g/c)\cos\theta, \qquad \nu = l,s \quad . \tag{1.29}$$

All that remains to close the model is to specify the f^{ν} functions that divide the bed weight between the large and small particles. Mathematically we have the constraint $f^{s} + f^{l} = 1$ $\forall\Phi^{s}$ and physically it follows that $f^{\nu}(\Phi^{\nu} = 0) = 0$ and $f^{\nu}\left(\Phi^{\nu} = 1\right) = 1$ must also hold.

Exercise 9: By considering $f^{l} = a_0 + a_1\Phi^{l} + a_2\left(\Phi^{l}\right)^2$ and $f^{s} = b_0 + b_1\Phi^{s} + b_2\left(\Phi^{s}\right)^2$ show that these constraints imply that $f^{s} = \Phi^{s} + B\Phi^{s}\left(\Phi^{s} - 1\right)$ where $B = b_2$. Note that the additional physical argument that the small particles are more likely to be falling implies $B > 0$.

Exercise 10: Using the mass balance equations (1.27) and the relationships for f^{ν} obtained above, derive equations for the evolution of the small particle volume fraction Φ^{s}. Assume small chute inclination such that $\sin\theta \approx 0$.

Writing the equation obtained in exercise 10 in dimensionless variables leads to a scalar conservation law for the small particle concentration $\Phi^{s} = \Phi(x,y,z,t) \in [0,1]$**,**

$$\frac{\partial\Phi}{\partial t} + \frac{\partial}{\partial x}(\Phi u) + \frac{\partial}{\partial y}(\Phi v) + \frac{\partial}{\partial z}(\Phi w) - S_r\left(\Phi(1-\Phi)\right) = 0\,, \tag{1.30}$$

where S_r is the non-dimensional segregation number. For the more general fluid saturated case (Thornton et al. 2006) $S_r = LB\hat{\rho}g\cos\theta/cHU$, where (as in section II) L,H,U are typical flow length, height, and down slope velocity scales; and, θ is the chute angle. The relative density

difference $\hat{\rho}$ is a dimensionless measure of the density contrast between the granular phase and the fluid phase (often air) that fills the interstitial pore space between the particles. The main weakness of this theory is that no model is provided for the overburden pressure on each constituent, but only a series of physical and mathematical constraints are derived. Thornton et al. (2006) then obtain the simplest function satisfying all constraints with *B* a free dimensionless constant, which appears in this function (exercise 9). Physically, *B* is a measure of the increased bed weight (overburden pressure) carried by the large particles compared to the small. Measuring pressure functions f^v directly in experiments is not easy, but these functions could be determined using particle-based simulations. These simulations are currently been carried out.

Taken the simple form for f^v, see exercise 9, the above segregation model gives very good agreement (using S_r as a fitting parameter) to both dry experiments performed by Savage and Lun (1988) and later, liquid saturated experiments of Vallance and Savage (2000). The model predicts the correct dependence of the segregation length (distance before the large and small particles are fully segregated) on the background fluid density, and that no segregation takes place if the particles and fluid are matched in density. The question of how to obtain the velocity field in the segregation model (1.30) is a challenge discussed in section IV.

IV. MAJOR CHALLENGES

In this section, we will pose several challenges concerning the relevance of idealized studies of shallow granular flow and depth-averaged modeling, and the scope of particle segregation models and multi-scale approaches to efficient and accurate modeling of shallow granular flows.

Firstly, the question is how relevant the detailed studies of granular flows under idealized conditions, as reviewed in section II, are to (dry) granular particle flows in the environment. In

contrast to the cases reviewed, dry particulate flows in nature consist of non-uniform and poly-dispersed particles over terrain of varying roughness. Furthermore, an interstitial fluid may be involved, for example when the soil of a hill or the rocky debris of a volcanic slope is saturated with water. The papers of Iverson and Denlinger (2001; and, Denlinger and Iverson 2001, 2004) focus more strongly on debris flows with an interstitial fluid. In their depth-averaged model, fluid and solid stress components are taken into account, but in the dry limit with only a solid fraction their model is closely related to (1.18) and (1.20). Their model contains an extra stress component in the x-y-direction, which concerns the internal friction angle and also uses the more complex Earth pressure coefficient K, i.e., (1.15). Additionally, extra nonlinear effects, due to the curvature of the bed, are taken into account but the basal friction coefficient is fixed to the tangent of the bed slope. One problem is, of course, that it is unclear what the dependence of the basal friction on the flow state is, e.g., on the instantaneous Froude number and the layer depth. The research reviewed indicates that basal friction must be variable as the flow changes from supercritical to subcritical. It remains a somewhat open question which effects are most important to forecast environmental particle flows. Dalbey et al. (2008) mention that granular flows are relatively insensitive to the internal friction angle, and the key parameters are the bed friction angle and the mass. They explored the input uncertainty with statistical methods and using a depth-averaged model similar to the one presented in II produced hazard maps indicating danger regions for geophysical granular mass flows.

Secondly, measurements indicate that the velocity of shallow granular flows is depth dependent (GDR MIDI 2004). Depth-averaged models keep only one degree of freedom in the vertical. When this restriction is too strong relative to the other approximations, it is useful to include some more degrees of freedom, as is done in Boussinesq water wave models. In addition,

the solid's volume fraction is variable, especially in the horizontal direction when flow changes from super- to subcritical or from fast thin to slow thick flows. The extension of shallow granular models to include horizontal variation of the solid's fraction while still keeping a limited number of degrees of freedom in the vertical is of particular interest.

Thirdly, particle size-segregation can have a major effect on the dynamics of shallow granular flows. Understanding this process is going to be a key step in improving the predictive power of existing models. There are two possible ways to couple the depth-averaged and segregation models. Fully three-dimensional velocity fields could be reconstructed from a depth-integrated avalanche theory and solved in conjunction with three dimensional segregation equations. When one depth-averages the equations of motion, a series of assumptions about the vertical dependence of flow variables are made. These assumptions can be used to reconstruct fully three-dimensional information from the two-dimensional depth-averaged theory and then employed in the three-dimensional segregation theory. A second approach is to depth-average the three-dimensional segregation equation (1.30) and then direct coupling with the bulk flow theory (1.18) is possible. The coupling of a segregation model with shallow-water theories is thus an open research question, which will lead to further investigation in next few years.

Finally, efficient DPMs would in principle eliminate the need to formulate continuum models altogether, but in practice this is impossible. In particular, the application of DPMs to flows with dead (static) and dynamic zones is of interest, in combination with formulating associated continuum models for shallow granular flow. Adequate determination of the normal and tangential coefficients of restitution is then required, yet efficient calculation of flows with non-uniform and poly-dispersed particles using DPMs is a challenge. New alleys of research are multi-scale modeling approaches (e.g., Van der Hoef et al. 2006). In these approaches macro-

scale continuum models are coupled with local (in time and space) DPMs, with the intention to save computational time.[1]

REFERENCES

Börzsönyi, T., Ecke, R.E. 2007. Flow rule of dense granular flows down a rough incline. Phys. Rev. E 76:031301.

Cooke, M. H., Stephens, D. J. & Bridgewater, J. 1976. Powder mixing - a literature survey. Powder Tech. 15:1–20.

Dalbey, K., Patra, A.K., Pitman, E.B., Bursik, M.I., Sheridan, M.F. 2008. Input uncertainty Input uncertainty propagation methods and hazard mapping of geophysical mass flows, J. Geophys. Res. 113, 05203.

Denlinger, R.P., Iverson, R.M. 2001. Flow of variably fluidized granular masses across three-dimensional terrain 2. Numerical predictions and experimental tests. J. Geophys. Res. 106:553–566.

Denlinger, R.P., Iverson, R.M. 2004. Granular avalanches across irregular three-dimensional terrain: 1. Theory and computation. J. Geophys. Res. 109, 01014.

GDR MiDi. 2004. On dense granular flows. Eur. Phys. J. E 14:341–365.

Gray, J.M.N.T., Tai, Y.-C., Noelle, S. 2003. Shock waves, dead zones and particle-free regions in rapid granular free-surface flows. J. Fluid Mech. 491:161–181.

Hákonardóttir, K.M., Hogg, A.J. 2005. Oblique shocks in rapid granular flows. Phys. Fluids 17: 077101.

van der Hoef, M.A., Ye M., van Sint Annaland, M. , Andrews IV, A.T., Sundaresan, S., Kuipers,

---

[1] We thank L. Courtland, V. Orgarko, S. Rhebergen and T. Weinhart for careful proofreading.

J.A.M. 2006. Multi-scale modeling of gas-fluidized beds. Adv. Chem. Eng. 31:65.

Iverson, R.M. 1997. The physics of debris flows. Reviews in Geophysics 35:245–296.

Iverson, R.M., Denlinger, R.P. 2001. Flow of variably fluidized granular masses across three-dimensional terrain 1. Coulomb mixture theory. J. Geophys. Res. 106:537–552.

Jenkins, J.T. 2006. Dense shearing flows of inelastic disks, Phys. of Fluids 18:103307.

Kerswell, R.R. 2005. Dam break with Coulomb friction: a model for granular slumping? Physics of Fluids 17: 057101.

Pouliquen, O., Forterre, Y. 2002. Friction law for dense granular flows: application to the motion of a mass down a rough inclined plane. J. Fluid Mech. 453, 133-151.

Pouliquen, O., Vallance, J.W. 1999. Segregation induced instabilities of granular fronts. Chaos 9, 621–630.

Savage, S.B. and Hutter, K. J.F.M. 1989. On the motion of a finite granular mass of material down a rough incline. 199:177-215.

Savage, S. B., Lun, C. K. K. 1988. Particle size segregation in inclined chute flow of dry cohesionless granular material. J. Fluid Mech. 189:311–335.

Thornton, A.R. Gray, J.M.N.T, Hogg, A. 2006. A three-phase model of segregation in granular avalanche flows. J. Fluid Mech. 550:1–25.

Vreman, A.W. , Al-Tarazi, M., Kuipers, J.A.M., van Sint Annaland, M., Bokhove, O. 2007. Supercritical shallow granular flow through a contraction: experiment, theory and simulation. J. Fluid Mech. 578:233–269.

Vallance, J.W., Savage, S.B. 2000 Particle segregation in granular flows down chutes. IUTAM Symp. on Segregation in Granular Materials (Eds. Rosato & Blackmore), pp. 31–51. Kluwer.